Applied Catalysis B: Environmental 226 (2018) 117–126

Contents lists available at ScienceDirect

Applied Catalysis B: Environmental

journal homepage: www.elsevier.com/locate/apcatb

Solvothermal synthesis of well-designed ceria-tin-titanium catalysts with enhanced catalytic performance for wide temperature NH_3-SCR reaction

Guodong Zhang, Weiliang Han, Haijun Zhao, Luyao Zong, Zhicheng Tang*

State Key Laboratory for Oxo Synthesis and Selective Oxidation, and National Engineering Research Center for Fine Petrochemical Intermediates, Lanzhou Institute of Chemical Physics, Chinese Academy of Sciences, Lanzhou, 730000, China

ARTICLE INFO

Keywords:
Solvothermal synthesis
Selective catalytic reduction
$CeSnTiO_x$
Synergistic interaction by Sn-Ce

ABSTRACT

Ternary mixed ceria-titanium catalysts doping tin were synthesized by a solvothermal method and applied to selective catalytic reduction (SCR) of NO with NH_3. The Sn doping catalyst showed better low-temperature activity compared with unmodified catalyst, which exhibited an extraordinarily wide operation window ranging from 180 to 460 °C and better the tolerance of H_2O or SO_2. Powder X-ray diffraction (XRD), laser Raman spectroscopy (Raman), fourier transform infrared spectroscopy (FTIR), X-ray photoelectron spectroscopy (XPS), transmission electron microscope (TEM), BET surface area by N_2-adsorption-desorption, hydrogen temperature-programmed reduction (H_2-TPR), ammonia temperature-programmed desorption (NH_3-TPD) were performed to study the structure, redox ability and surface acidity for the $CeSnTiO_x$ catalyst. Notably, the addition of Sn could prominently modify and optimize the structure of mixed metal oxides. Meanwhile, it was verified that synergistic interaction between of Ce and Sn surprisingly produced, and crystal defects, oxygen vacancies, acid sites as well as the specific surface areas evidently increased. In addition, the uniform pore channel was also beneficial to NH_3-SCR. Especially, the electron interaction between Sn and Ce in reaction could greatly improve the SCR performance and H_2O/SO_2 durability.

1. Introduction

Owing to the global scale of atmospheric pollution and climate warming arising from greenhouse gas emission (such as NO_x, SO_2 and so on) generated by the use of fossil fuels, there is a need to effectively eliminate nitrogen oxides for addressing environmental issues and sustainable development [1–3]. Numerous techniques have been utilized to relief and eliminate the pollution from fossil fuel. Among these technologies, the SCR was considered as one of promising remedies [4–6]. Notably, V_2O_5-WO_3 (MoO_3)/TiO_2 catalyst has been treated as a representative commercial SCR catalyst to eliminate the exhaust gas from power plants. Nevertheless, this catalyst could not be applied to remove NO_x from flue gases of other industries, such as steel, glass and so on, due to operating at relatively high and narrow temperatures window (320–420 °C). In addition, vanadium catalysts are prohibited from application by legislation in many developed countries on account of biological toxicity. Therefore, it is desirable and urgent to develop environmental friendly de-NOx catalysts with low-temperature operating regions.

Non-vanadium denitrated catalysts have been extensively studied in recent years, including transition metal oxide and rare earth metal oxide catalysts [7–9]. Therein, rare earth metal oxide catalysts have been widely explored owing to eco-friendly, inexpensive and abundant reserves [10,11]. Particularly, cerium-based catalysts have attracted more and more attention because of some distinctive chemical features such as oxygen storage capacity and redox properties [8,9]. Therefore, Ce-based catalysts have been reported plentifully by researcher for the SCR [12–14]. However, Ce-based catalyst scarcely applied as a commercial catalyst owning to poor thermal stability and weak anti-sulphur properties [15,16]. In order to solve the above problems, one of the effective strategies is to optimize Ce dispersion through the modulation of support on carrier channel as much as possible. Many materials could be used as carrier, such as mesoporous carbon, expanded clay and so on [17–19]. It is most suitable and low-costing that titanium dioxide was considered as an important carrier to deal with industrialized exhaust gas for SCR catalyst. TiO_2 could not only provide higher surface area and pore volume for the catalytic active center, but also supply abundant acid sites [20,21]. Generally, the SCR catalysts was prepared by impregnation, which exhibited poor performance attributing to the low surface area and concentrated activity center in SCR reaction. Hence, it is necessary to develop ceria-titanium catalyst with desirable catalytic activity via adjusting synthesis method or doping other elements.

* Corresponding author.
E-mail address: tangzhicheng@licp.cas.cn (Z. Tang).

https://doi.org/10.1016/j.apcatb.2017.12.030
Received 13 July 2017; Received in revised form 11 December 2017; Accepted 12 December 2017
Available online 13 December 2017
0926-3373/

According to previous reports [13,22], it is easy to obtain the superior dispersion by co-precipitation and sol-gel method. The deficiency of the method is obvious, such as complex process and requiring excessive precipitant or organic matter. There is an efficient and facile strategy that heat synthesis method could decompose various metal salts and form metal oxides, which possessed smaller grain size. Herein, it is extensively noticed and studied that the homogeneous metal oxides were prepared in the solvent heat reaction. Mesoporous ceria-titanium catalyst was reported using one pot hydrothermal method in our previous work [23], which showed excellent activity for NO conversion, a wider operating temperature range and preferable resisting H_2O. Nonetheless, it is discovered that the poor resistance of SO_2 limited the application of mesoporous ceria-titanium catalyst due to a single active component.

Little crystalline grain generated is rarely reported via solvent thermal synthesis method, which implied that each of the components is mixed uniformly, and it can not only improve the surface area, but also promote the synergetic interaction among the ingredient of the catalyst. SnO_2 as an n-type semiconducting metal oxide possesses wide band gap, intrinsic defects and oxygen vacancies [24–26]. It is generally gained attention and applied to the gas sensors, transparent conductors and catalysis yield [27,28]. A series of Ce_xSn_y catalysts reported by Li et al. were prepared with the inverse co-precipitation method and showed a high-efficiency for NH_3-SCR reaction [29]. It is concluded that introduction of SnO_2 increased amount of chemisorbed oxygen and was beneficial to improve SCR activity. It is still urgent to further improve the uniformity of composition and low-temperature activity through co-precipitation method. The $CeSnTiO_x$ catalyst prepared by solvothermal method is expected to achieve the larger specific surface areas, uniform composition, abundant crystal defects and oxygen vacancies, and then improved the SCR performance by electron interaction between Sn and Ce in reaction.

In this paper, SnO_2 was doped in ceria-titanium catalyst by a solvothermal method and compounded ternary mixed metal oxide. H-$CeSnTiO_x$-E catalyst was easy to be synthesized and exhibited high NO conversion, a wider operating temperature range and admirable resistance of H_2O or SO_2, which could be treated as a promising candidate to eliminate nitrogen oxides.

2. Experimental

2.1. Sample preparation

H-$CeSnTiO_x$-E (Ce: Sn: Ti = 1:1:5) was synthesized via a solvothermal method, which had been described in detail in our previous studies [23]. Schematic diagram of preparation was shown in Fig. 1. For the sake of clarity, the chemical characteristics (such as composition, preparation method and solvent) of all samples were summarized in Table 1. In a typical synthesis process, 1.2 g of urea and 1.16 g of $(EO)_{20}(PO)_{70}(EO)_{20}$ triblock copolymer (Pluronic P123, M_n = 5800, Sigma Aldrich) was dissolved in 20.0 mL of ethyl alcohol with vigorous stirring, which was labeled A solution. Then, 5.67 g of tetrabutyl titanate (Sinopharm Chemical Reagent Co., Ltd., China) was added into a mixed aqueous solution with 20.0 mL of ethanol and 1.0 mL of hydrochloric acid under magnetic stirring, 1.45 g of $Ce(NO_3)_3{\cdot}6H_2O$ (Sinopharm Chemical Reagent Co., Ltd., China) and 0.75 g of $SnCl_2{\cdot}2H_2O$ (Sinopharm Chemical Reagent Co., Ltd., China) were dissolved into the above solution under magnetic stirring, Ce:Sn:Ti = 1:1:5 in molar ratio, which was labeled B solution. The A and B solutions were transferred into a 100 mL PTFE (polytetrafluoroethylene) autoclave and placed in an oven. The temperature maintained at 80 °C for 48 h, and was increased to 120 °C for 5 h. Finally, the products were washed three times using deionized water, and dried at 100 °C overnight. The samples were calcined at 400 °C for 3 h (2 °C min^{-1}) in air.

Table 1
The chemical characteristics of all samples.

Catalyst	Composition	preparation method	Solvent (alcohol)
H-$CeTiO_x$-E	CeTi = 1:5	solvothermal	ethyl
H-$SnTiO_x$-E	Sn:Ti = 1:5	solvothermal	ethyl
H-$CeWTiO_x$-E	Ce:W:Ti = 1:1:5	solvothermal	ethyl
H-$CeSnTiO_x$-E	Ce:Sn:Ti = 1:1:5	solvothermal	ethyl
H-$CeSnTiO_x$-M	Ce:Sn:Ti = 1:1:5	solvothermal	methyl
H-$CeSnTiO_x$-P	Ce:Sn:Ti = 1:1:5	solvothermal	n-propyl
H-$CeSnTiO_x$-B	Ce:Sn:Ti = 1:1:5	solvothermal	n-butyl

For comparison, Ce: Ti = 1:5 in molar ratio was labeled H-$CeTiO_x$-E, similarly H-$SnTiO_x$-E (Sn: Ti = 1:5) and H-$CeWTiO_x$-E (Ce: W: Ti = 1:1:5) were synthesized in accordance with the above approach. The final mesoporous materials were labeled with the general form H-$CeSnTiO_x$-Y, Y stands for different of solvent, for instance, H-$CeSnTiO_x$-M, H-$CeSnTiO_x$-P and H-$CeSnTiO_x$-B referred to methyl alcohol, n-propyl alcohol and n-butyl alcohol as solvent.

2.2. Analytical instrumentation

X-ray diffraction (XRD) analysis measurements were carried out and recorded on a Rigaku D/MAX-RB X-ray diffractometer with a target of Cu Kα operated at 60 kV and 55 mA with a scanning speed of 5° min^{-1} ranged from 5 to 80°. Laser Raman spectroscopy (LRS) was tested on a RM 2000 microscope confocal Raman spectrometer (Renishaw PLC) with 514 nm. Transmission electron microscope (TEM) was investigated

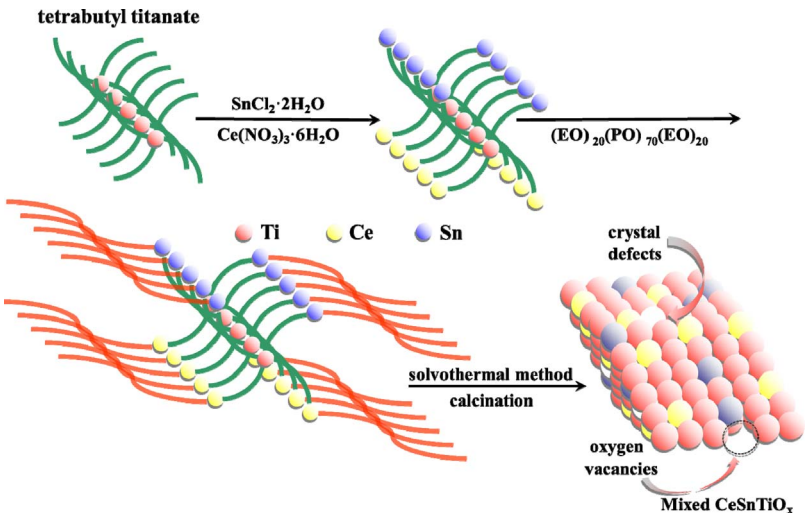

Fig. 1. Schematic diagram of preparation and structure.

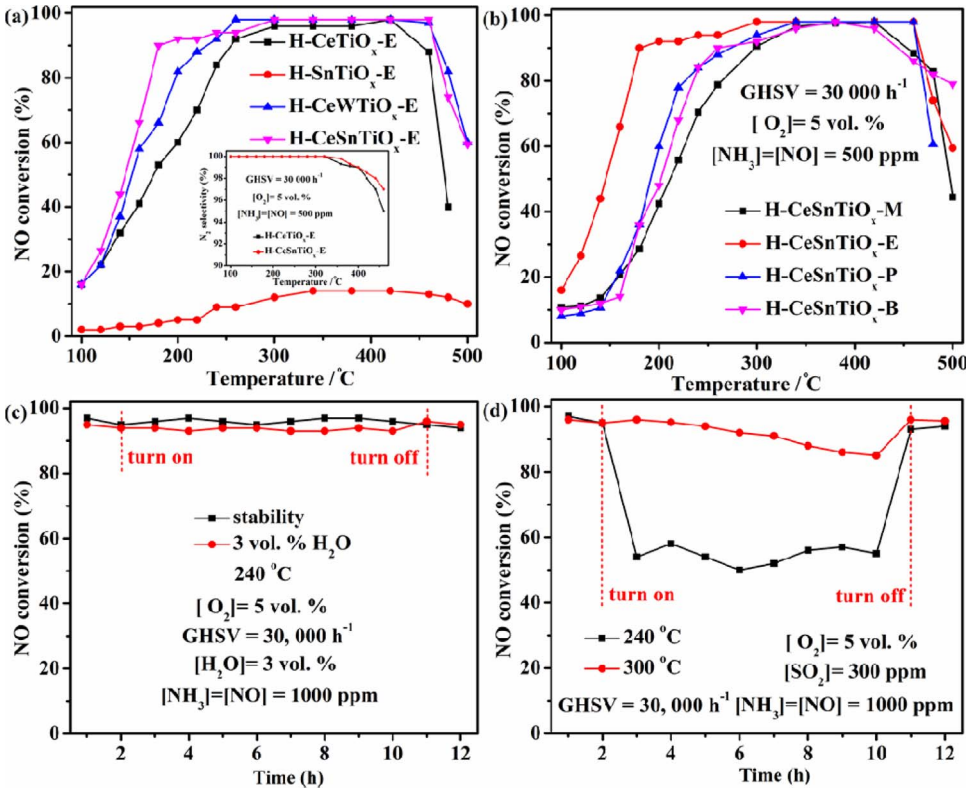

Fig. 2. NO conversion of the catalysts and N_2 selectivity (inset) during the NH_3-SCR reaction over the H-CeTiO_x-E and H-CeSnTiO_x-E catalysts (a), the H-CeSnTiO_x-Y catalysts (b), stability and H_2O tolerance test of the H-CeSnTiO_x-E catalyst (c), SO_2 resistance study of the H-CeSnTiO_x-E catalyst at 240 and 300 °C (d), 5% O_2, GHSV = 30, 000 h^{-1}.

on a JEOL JEM-2010 transmission electron microscope equipped at 200 kV. N_2 adsorption– desorption isotherms were obtained at 77.3 K using a Micromeritics ASAP 2020 instrument and based on six measurements at relative pressures of N_2 in the range of 0.05–1.00. X-ray photoelectron spectroscopy (XPS) were recorded on a VG ESCALAB 210 Electron Spectrometer (Mg Kα radiation, hν = 1253.6 eV). XPS data were calibrated using the binding energy of C 1s (BE = 284.6 eV) as the standard. The temperature programmed reduction with hydrogen experiment (H_2-TPR) was performed by DAS-7000 automatic multifunction adsorption apparatus. The reducing gas consists of 5 vol.% H_2 and 95 vol.% N_2 with the 30 mL min^{-1} flow. The quartz tube reactor was loaded with in powder form. The test was carried out with 50 mg sample range from 50 to 800 °C at a heating rate of 10 °C min^{-1}. The test conditions of NH_3-TPD are similar to that of H_2-TPR. The adsorbing gas was 5 vol.% NH_3 balanced by N_2 and the sample was 100 mg. The sample was purged with N_2 gas at 300 °C for 1 h before the test. FTIR measurements (4000–400 cm^{-1}) were obtained with a Thermo NEXUS 870 equipment, with a resolution of 4 cm^{-1}.

2.3. Catalytic activity measurements

The SCR activity evaluation was performed in a fixed-bed reactor using 0.4 or 0.12 mL (approximately 0.4 or 0.12 g) of the catalysts, when using 0.4 mL (0.12 mL) of the catalysts, gas hourly space velocity (GHSV) value was 30, 000 h^{-1} (100, 000 h^{-1}). The following reaction conditions were used: 500 or 1000 ppm NO, 500 or 1000 ppm NH_3, 5 vol% O_2, 300 ppm SO_2 (when used), 3 or 9 vol% H_2O (when used) and balance N_2 and the total flow rate was 200 mL min^{-1}. The concentrations of NO in the inlet and outlet gas were tested by a KM9106 flue gas analyzer. The concentrations of N_2O were tested by a G200 analyzer. The NO percent conversion and the N_2 selectivity were calculated according to the following expression [23,24]:

$$\text{NO conversion}(\%) = \frac{[NO]_{inlet} - [NO]_{outlet}}{[NO]_{inlet}} \times 100\% \quad (1)$$

$$N_2\ \text{selectivity}(\%) = \left(1 - \frac{2[N_2O]_{outlet} - [NO_2]_{outlet}}{[NO]_{inlet} - [NH_3]_{inlet}}\right) \times 100\% \quad (2)$$

Where $[NO]_{inlet}$ indicates the inlet NO concentration at steady state and $[NO]_{outlet}$ indicates the sum concentration of outlet NO. In the SCR reaction, the related reactions to N_2 selection are summarized [30–32]:

$$4NH_3 + 4NO + O_2 \rightarrow 4N_2 + 6H_2O < 1 >$$

$$NO + O^* \rightarrow NO_2 < 2 >$$

$$4NH_3 + 2NO_2 + O_2 \rightarrow 3N_2 + 6H_2O < 3 >$$

$$2NH_3 + 2NO_2 + NO \rightarrow 2N_2 + 3H_2O < 4 >$$

$$4NH_3 + 4NO + 3O_2 \rightarrow 4N_2O + 6H_2O < 5 >$$

A relative turnover frequency (TOF) value was used to evaluate the catalytic velocity for samples. The TOF value of NO over active centre Ce was calculated by the following formula [23–25]:

$$\text{TOF} = \frac{(P\nu/RT)\alpha}{m_{cat}\beta_{Ce}/M_{Ce}} \quad (3)$$

Where P is 1.01 MPa, ν is the flow rate of NO (0.1 mL min^{-1}), R is 8.314 J mol^{-1} K^{-1}, α is the NO conversion (%), m_{cat} is the mass (0.4 g), β_{Ce} is the Ce loading calculated using the XPS data (%) and M_{Ce} is the molar mass (140.1 g mol^{-1}). Test temperature point at 373, 393, 413, 433 and 453 K, respectively.

3. Results and discussion

3.1. Catalysts characterization

H-CeTiO_x-E, H-SnTiO_x-E, H-CeWTiO_x-E and H-CeSnTiO_x-E catalysts were measured for NH_3-SCR ranging 100–500 °C, as shown in Fig. 2(a). The NO conversion was less than 18% for the H-SnTiO_x-E catalyst in the whole temperature range, which illustrated SnO_2 could be hardly regarded as active center for the SCR reaction. For the H-CeTiO_x-E

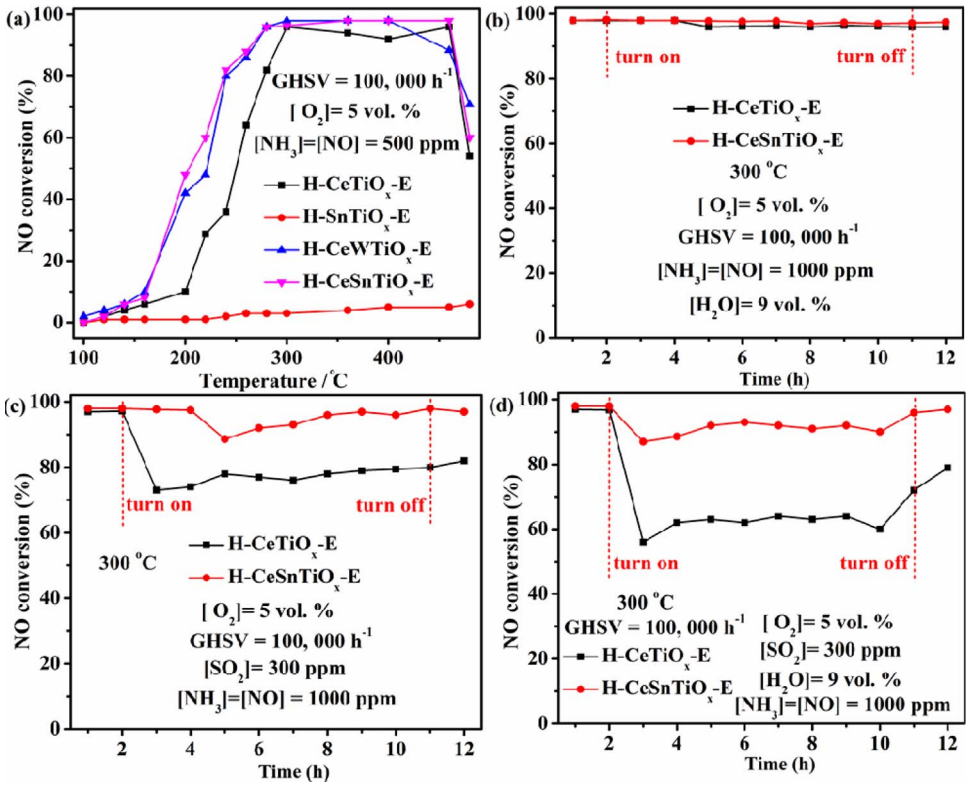

Fig. 3. NO conversion of the catalysts (a), H_2O tolerance test (b), SO_2 tolerance test (c), both H_2O and SO_2 tolerance test (d) of the H-CeTiO$_x$-E and H-CeSnTiO$_x$-E catalysts at 300 °C, 5% O_2, GHSV = 100, 000 h^{-1}.

catalyst, the NO conversion was 90% ranging from 260 °C to 380 °C under a GHSV of 30, 000 h^{-1}, while the H-CeWTiO$_x$-E catalyst showed a conversion more than 90%. The result indicates that WO_3 doping catalyst presented preferable low-temperature SCR activity, which was consistent with the previous reports [22,33], accounting for the increasing of active Ce^{3+} relative amount, the enhanced synergistic effect of components and surface acid sites. Noticeably, the H-CeSnTiO$_x$-E catalyst showed a better low-temperature activity, compared with the H-CeWTiO$_x$-E catalyst. The NO conversion achieved 90% from 180 to 460 °C under the same GHSV. The N_2 selectivity has been slightly improved, comparing with the absence of Sn (Fig. 2(a) inset). N_2 selectivity of the H-CeSnTiO$_x$-E catalyst exceeded 98% ranging from 100 to 400 °C. These results suggested that the low-temperature activity was drastically promoted owing to the appropriate introduction of tin into the mesoporous ceria-titanium catalyst. It might be prominently modified and optimized the structure of metal oxide, strengthened the synergistic effect of metal particles, and improved Brønsted acid sites, which was favorable to NO conversion for the low-temperature SCR reaction.

The influence of different solvents on catalyst activity showed in Fig. 2(b), and the SCR performance was exhibited in the following order: H-CeSnTiO$_x$-E > H-CeSnTiO$_x$-P > H-CeSnTiO$_x$-B > H-CeSnTiO$_x$-M. Solvent had a crucial influence on the formation of the H-CeSnTiO$_x$-Y catalysts, which affected the activity of catalyst. It was not conducive to the formation of the ternary mixed metal oxide that the boiling point was too low or too high of solvent (Table S1†) and ethanol as the solvent was benefit to efficient catalyst in this study.

3.2. Stability, H_2O or SO_2 resistant properties

In the process of practical application, smoke relatively keeps low temperature and high concentration of NO from factories. The optimal H-CeSnTiO$_x$-E catalyst was examined at 240 °C under a GHSV of 30, 000 h^{-1}, a relatively high concentration of NO (1000 ppm), which achieved more than 95% NO conversion and shown in Fig. 2(c). In addition, there was some fraction of water vapor in the exhaust gas that has a negative effect in flue gas on the catalytic activity. Fig. 2(c) showed the NO conversion over the H-CeSnTiO$_x$-E catalyst as a function of time in the presence of 3% vol. H_2O at 240 °C under the same GHSV. The NO conversion over the H-CeSnTiO$_x$-E catalyst had a negligible decline during the whole H_2O tolerance test, indicating that the H-CeSnTiO$_x$-E catalyst resisted the poison of H_2O at the test conditions. It is obviously that the NO conversion of the H-CeSnTiO$_x$-E catalyst recovered after turning-off the water vapor, implying the active sites was poisoned and probably activation of reactant were depressed.

Because most of the air pollution from factory contains a large number of sulfur dioxide, the resistance of SO_2 of the SCR catalyst is a vitally important factor for its scale application. As shown in Fig. 2(d), the H-CeSnTiO$_x$-E catalyst was examined at 240 and 300 °C, which exhibited clear distinction. The NO conversion changed from 95 to 54% at 240 °C as soon as turning on the 300 ppm concentration of SO_2, while that gradually fallen as a function of time at 300 °C and reached 85% after 8 h of toleration of SO_2 test. After turning-off the SO_2, the activity recovered to 93%, suggesting that the catalyst has not been completely poisoned and sulfur dioxide might be preferentially adsorbed on the active or acid sites and NH_3 could not participate in the reaction. It is concluded that the H-CeSnTiO$_x$-E catalyst has satisfactory resistance to H_2O or SO_2 poisoning. It is worth noting that the catalytic performance of ceria-titanium catalyst was obviously enhanced via modifying with appropriate tin, compared with our previous work [23].

3.3. Activity, H_2O and SO_2 resistant properties at high GHSV

Furthermore, to assess performance of the catalysts under the nearly practical industrial conditions, the H-CeWTiO$_x$-E, H-SnTiO$_x$-E, H-CeTiO$_x$-E and H-CeSnTiO$_x$-E samples were tested under a high GHSV of 100, 000 h^{-1} and the results showed in Fig. 3(a). The H-CeSnTiO$_x$-E catalyst exhibited more than 80% NO conversion ranging from 240 to 460 °C and the NO conversion was increased to 40% at 240 °C, compared with H-CeTiO$_x$-E. In addition, the H-CeSnTiO$_x$-E catalyst was valued at 300 °C under a GHSV of 100, 000 h^{-1} with 9% vol. H_2O, which exerted more than 95% NO conversion as shown in Fig. 3(b).

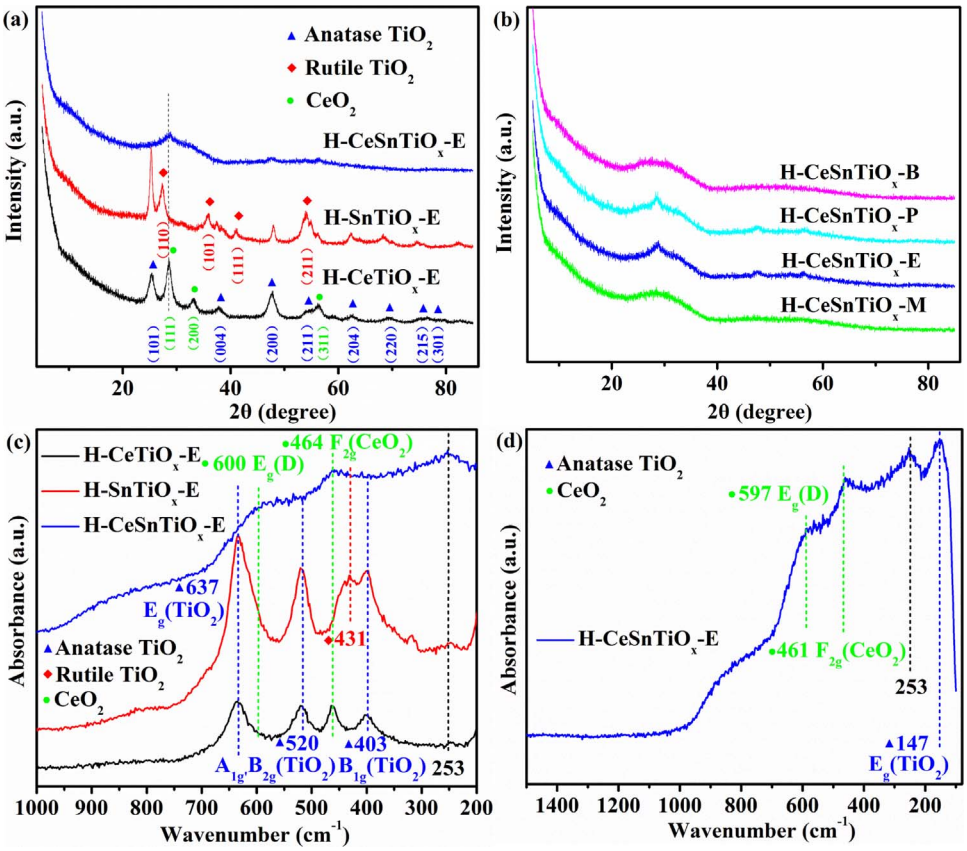

Fig. 4. XRD patterns of the H-CeTiO$_x$-E, H-SnTiO$_x$-E, H-CeSnTiO$_x$-E catalysts (a), H-CeSnTiO$_x$-M, H-CeSnTiO$_x$-E, H-CeSnTiO$_x$-P, H-CeSnTiO$_x$-B catalysts (b) and Raman spectroscopy of the H-CeTiO$_x$-E, H-SnTiO$_x$-E, H-CeSnTiO$_x$-E catalysts (c), the enlargement of H-CeSnTiO$_x$-E catalyst (d).

When 300 ppm concentration of SO_2 was introduced into the mixing gas, the NO conversion maintained 90% for the H-CeSnTiO$_x$-E catalyst (Fig. 3(c)). What's more, there exists a mass of NO, SO_2 and H_2O simultaneously in exhaust gas from some industries. Hence, both SO_2 and H_2O durability was further investigated in Fig. 3(d). When SO_2 and H_2O were simultaneously introduced into the reactor, the NO conversion of the H-CeTiO$_x$-E catalyst had a decrease from 96.8% to 56%, while that of the H-CeSnTiO$_x$-E catalyst reduced 10% and recovered 95% after turning off SO_2 and H_2O, indicating that the H-CeSnTiO$_x$-E catalyst might be a promising candidate for NO_x removal at low temperature in real applications. These results illustrated that the proper addition of Sn could effectively improve H_2O and SO_2 resistant.

3.4. Structure of the catalyst

Fig. 4(a) showed the XRD results of the H-CeTiO$_x$-E, H-SnTiO$_x$-E and H-CeSnTiO$_x$-E catalysts. For the H-CeTiO$_x$-E catalyst, all of the peaks could be assigned to anatase titanium structure of TiO_2 (JCPDS card no. 71- 1168) and CeO_2 (JCPDS card no. 34- 0394), which was similar to previous literatures [23,34]. The average size of the crystalline TiO_2 was calculated at 4.7 nm by Scherrer's formula [22]. It was smaller than our previous report [23], meaning that solvent played a crucial factor in controlling crystal growth and affecting activity of catalysts. For the H-SnTiO$_x$-E catalyst, there were not any peaks that could be ascribed to SnO_2. Interestingly, the peaks at 27.3°, 35.9°, 41.0° and 54.0° were surveyed, which can be indexed to the TiO_2 (110), (101), (111) and (211) lattice planes of rutile titanium structure of TiO_2 (JCPDS card no. 76- 1940). It illustrated that Sn doped into the structure of the TiO_2, which was consistent with Berlinguette's report [33,35]. Analogically, the average crystallite size of SnTiO$_x$ increased to 21.4 nm, suggesting that some crystallites with Sn—O—Ti structures might be formed and promoted the growth of the binary metal-oxide nanostructure. Finally, the peaks of CeO_2 became broader and the intensity became lower compared with that of the H-CeTiO$_x$-E catalyst. Furthermore, little crystalline phase in the H-CeSnTiO$_x$-E catalyst was ascribed to anatase or rutile titanium, implied that cerium oxide existed as highly dispersed species. In other words, the homogeneous phase contained together TiO_2, SnO_2 and CeO_2 phases, some crystallites with Sn—O—Ti and Sn—O—Ce structures might also be formed, due to some diffraction peaks were assigned to TiO_2, SnO_2 and CeO_2 in the positions of the broad bumps. To the best of our knowledge, using solvent thermal synthesis method for the mixed metal oxide has scarcely been reported in the field of catalysis.

As shown in Fig. 4(b), the obvious feature peaks of CeO_2 was exhibited for the H-CeSnTiO$_x$-E and H-CeSnTiO$_x$-P catalysts while little characteristic crystalline phase of CeO_2 was observed in the H-CeSnTiO$_x$-B and H-CeSnTiO$_x$-M catalysts. CeO_2 play a key role in the process of the SCR reaction, such as $4Ce^{4+} + O^{2-} \rightarrow 4Ce^{4+} + 2e^- + 0.5O_2 \rightarrow 2Ce^{4+} + 2Ce^{3+} + 0.5O_2$ and $2Ce^{4+} + Sn^{2+} \leftrightarrow 2Ce^{3+} + Sn^{4+}$. So the performances decreased in the order: H-CeSnTiO$_x$-E > H-CeSnTiO$_x$-P > H-CeSnTiO$_x$-B > H-CeSnTiO$_x$-M.

In regard to the crystalline structure of the catalysts, more information was investigated by the Raman spectroscopy (Fig. 4(c)), which could be regarded as a complementary characterization of XRD. Obviously, the structure of TiO_2 and CeO_2 were examined for the H-CeTiO$_x$-E catalyst, while the peak of TiO_2 became wider and stronger for the H-SnTiO$_x$-E catalyst, suggesting that the Sn atoms incorporated into the crystal lattice of TiO_2 and increased concentration of crystal defects. For the H-CeSnTiO$_x$-E catalyst, the weak peaks located at around 147 and 461 cm^{-1} were assigned to the B_{1g} (TiO_2) and F_{2g} (CeO_2) [28,30], respectively, illustrating that Sn—O and Ce—O structures existed. Furthermore, the shifting and broadening peaks might be the presentence of oxygen vacancies due to a change of CeO_2 environment, which suggested that Ti or Sn doped into the crystal lattice of ceria. The existence of oxygen vacancies and sublattice distortions could be detected frequently by Raman spectroscopy in ceria-based materials. The bands around 253 and 600 cm^{-1} were related to oxygen vacancies which could improve oxygen storage and increased the

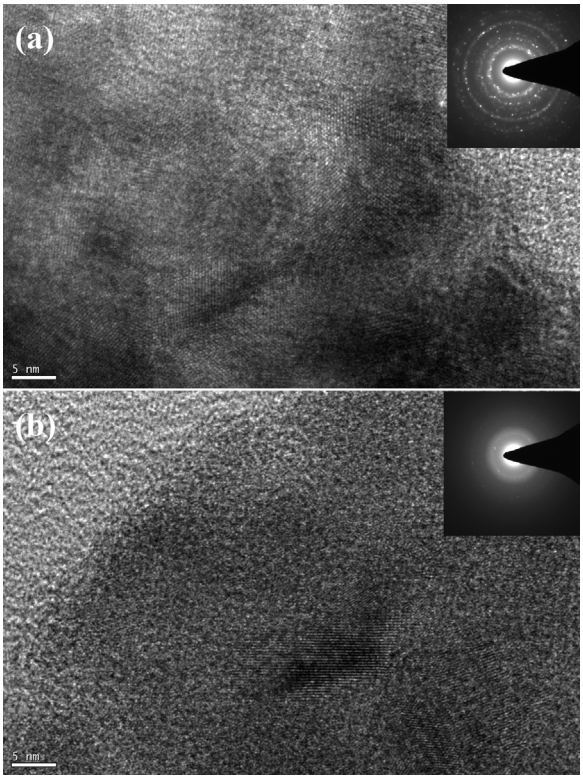

Fig. 5. HRTEM image of the H-SnTiO$_x$-E (a) and H-CeSnTiO$_x$-E (b) catalysts.

transformation frequency between Ce^{3+} and Ce^{4+} [36]. Therefore, the H-CeSnTiO$_x$-E catalyst had the superior redox ability that facilitated NO oxidation and benefited to "fast SCR" reaction.

In order to further certify the structural analysis, the morphology of the H-SnTiO$_x$-E and H-CeSnTiO$_x$-E catalysts were investigated by TEM, as shown in Fig. 5. For the H-SnTiO$_x$-E catalyst, the block particles were detected and the diameter was larger than 20 nm, which was consistent with the XRD results. The result of Fig. 5(a) revealed that the width of the diffraction peak was 0.35 nm, indicating that binary metal oxide was more likely to grow into larger particles and obtained higher crystallinity under the condition of solvent thermal synthesis method. On the contrary, for the H-CeSnTiO$_x$-E catalyst, there was only a crystal particle that size was about 5 nm in Fig. 5(b) and interplanar distances size was about 3.17 nm (Fig. S1†) which was greater than CeO_2 (3.12 nm), illuminating that a small quantity of Sn or Ti doping into the lattice of CeO_2. It could increase crystal defects and enhance the interaction of components. Moreover, any diffraction peak had not been observed in the inset of Fig. 5(b). Interestingly, the process of crystalline grains growth were notably inhibited when tin was added, which meant TiO_2, SnO_2 and CeO_2 dispersed within the ternary system of mixed metal oxide.

Not only crystal defects and oxygen vacancies increased, but also the specific surface area was improved and porous structure was optimized after doping Sn, which could be further demonstrated by the nitrogen adsorption and desorption isotherms at 77.3 K and the results were shown in Fig. 6(a). The H-CeTiO$_x$-E and H-SnTiO$_x$-E catalysts were defined as type III and type H1 according to IUPAC classification, which might be the characteristic feature of mesoporous structure and accumulated channel. For the H-CeSnTiO$_x$-E catalysts, it was ascribed to a H1 isotherm of type I and the nitrogen adsorption and desorption curve improved slowly in the relative pressure range from 0.3 to 0.95, indicating that the uniform micro- and mesoporous structure existed. The information of the specific surface area and pore volume of these catalysts were also listed in Table 2. The BET surface areas of the H-CeTiO$_x$-E, H-SnTiO$_x$-E and H-CeSnTiO$_x$-E catalysts were 87.79, 14.80 and 133.64 $m^2 g^{-1}$, respectively. The H-CeSnTiO$_x$-E catalyst possessed higher specific surface area than that of others, suggesting that the structure was obviously modified and optimized via adding suitable amount of tin. Furthermore, the pore size distribution curves of the catalysts were described and shown in Fig. 6(b). There existed a few of pore channel on the surface of the H-SnTiO$_x$-E catalyst while much lower than that of the H-CeTiO$_x$-E catalyst, and the pore channel concentrated range from 2 to 8 nm. More importantly, the pore size of the H-CeSnTiO$_x$-E catalyst exhibited better uniform than others, distributed on 2–4 nm, suggesting that uniform and appropriate pore sizes were beneficial to SCR reaction [37,38].

Therefore, it was obvious that the mixed metal oxide structure were prominently modified and optimized, such as homogeneous distribution of the components, increased crystal defects and oxygen vacancies, the larger specific surface areas and uniform pore channel, which were benefiting to SCR reaction.

3.5. Catalysts reducibility

It was significant to discuss the reducibility of the catalysts, which were verified by H_2- TPR while SCR reaction was closely related to reducing property and the results were exhibited in Fig. 7(a). The peak around 340 °C was attributed to the partial reduction of Sn^{4+} to Sn^{2+} state. The strongest and widest peak appeared in the range of 550–800 °C, which was assigned to a major reduction peak of Sn^{2+} to Sn^{4+} and might be completely reduced to the metal Sn [28]. There were three peaks the reduction of surface oxygen of CeO_2, ceria of type Ce^{4+}—O—Ce^{4+} and Ce^{3+}—O—Ce^{4+} could be obviously surveyed on H-CeSnTiO$_x$-E catalyst [13,39,40]. The peak range from 220 to 420 °C was assigned to the reduction of surface oxygen and partial Sn^{4+} to the Sn^{2+} state, indicating that abundant O_α and active Sn^{4+} species existed in the H-CeSnTiO$_x$-E catalyst. It was clear that surface oxygen increased and the interaction between CeO_2 and SnO_2 strengthened after doping tin. The peak around 576 °C was lower than typical reduction of Ce^{4+} to the Ce^{3+} state, implying dispersed CeO_2 with admirable redox ability. The finally peak at 665 °C was ascribe to reduction of Sn^{2+} and Sn^{4+} to the metal Sn and shifted to the lower temperature than that of the H-SnTiO$_x$-E catalyst. Hence, the H-CeSnTiO$_x$-E catalyst performed better redox properties and the interoperable effect of metal particles, which could be demonstrated by XPS spectra and favorable to"fast-SCR" reaction.

The chemical states and relative quantities of elements in the near-surface region were detected to XPS spectra for the catalysts. The surface atom ratios of the catalysts were summarized in Table 3. Fig. 7(b) showed the XPS spectra of Ce 3d can be divided into eight characteristic peaks labeled as v (882.60 eV), v′ (885.80 eV), v″ (889.40 eV), v‴ (898.45 eV), u (900.90 eV), u′ (903.95 eV), u″ (907.94 eV), u‴ (916.90 eV). The Ce^{4+} was the primary valence state and a small amount of Ce^{3+} co-exists of Ce for the H-CeTiO$_x$-E catalyst. The amounts of Ce^{3+} species can be calculated on basis of the area ratio, relative to total $Ce^{3+}/(Ce^{4+} + Ce^{3+})$ was 22.04% for the H-CeTiO$_x$-E catalyst. Meanwhile, the peak of Ce^{3+} was broader and higher for the H-CeSnTiO$_x$-E catalyst, the $Ce^{3+}/(Ce^{4+} + Ce^{3+})$ ratio was 31.19%, which was higher than that of the H-CeTiO$_x$-E catalyst, indicating that the active Ce^{3+} species increased by doping Sn. The higher $Ce^{3+}/(Ce^{4+} + Ce^{3+})$ ratio meant the conversion between Ce^{4+} and Ce^{3+} could be more frequently as well as the generation of more active surface oxygen (O_α) [41,42], which accorded with follows:

$4Ce^{4+} + O^{2-} \rightarrow 4Ce^{4+} + 2e^- + 0.5O_2 \rightarrow 0{\cdot}5O_2 \rightarrow$

$2Ce^{4+} + 2Ce^{3+} + 0.5O_2$. Furthermore, the higher Ce^{3+} ingredient could be advantageous to comparatively high mobility of active oxygen species, illustrating that the H-CeSnTiO$_x$-E catalyst might be better reducibility property.

The O 1s XPS spectra of the H-CeTiO$_x$-E, H-SnTiO$_x$-E and H-CeSnTiO$_x$-E catalysts were fitted by the aforementioned procedure and results were shown in Fig. 7(c). $O_\alpha/(O_\alpha + O_\beta)$ ratio was in the

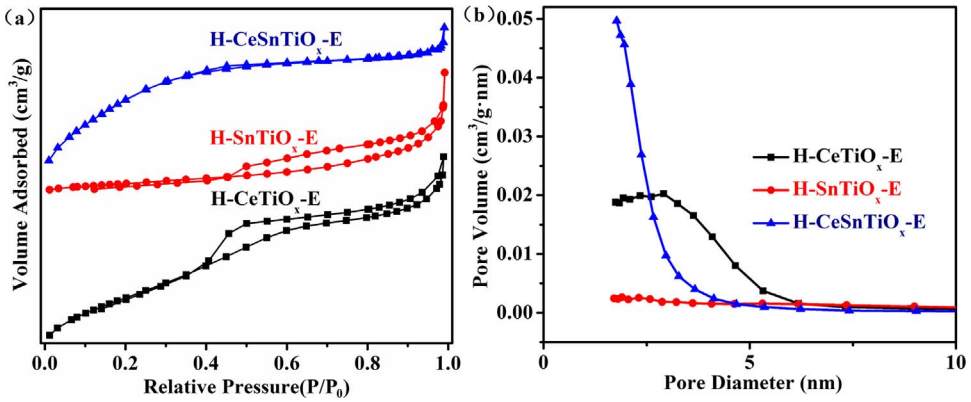

Fig. 6. N_2 adsorption-desorption isotherms of the catalysts measured at 77.3 K (the adsorption isotherm is labeled with filled symbols) (a), pore size distribution.

Table 2
Surface area, pore characteristics and average TiO_2 crystallite size of the H-CeTiO$_x$-E, H-SnTiO$_x$-E and H-CeSnTiO$_x$-E catalysts.

Catalyst	BET surface are ($m^2\,g^{-1}$)	Pore volume ($cm^3\,g^{-1}$)	Pore size (nm)	Crystal size (nm)
H-CeTiO$_x$-E	87.79	0.08	3.71	4.7
H-SnTiO$_x$-E	14.80	0.03	7.95	21.4
H-CeSnTiO$_x$-E	133.64	0.08	2.28	–

following order: H-SnTiO$_x$-E (28.26%) < H-CeTiO$_x$-E (30.14%) < H-CeSnTiO$_x$-E (46.66%). Obviously, H-CeSnTiO$_x$-E possessed more O_α ascribed to the introduction of tin. Furthermore, according to previous reports [34,43,44], a high $O_\alpha/(O_\alpha + O_\beta)$ ratio was favorable for NO oxidation and accelerated the "fast SCR" reaction at low temperature. Then, the above assumption confirmed that the desirable performance at low temperature was attributed to the intrinsic defects and the presence of abundant oxygen vacancies for the H-CeSnTiO$_x$-E catalyst.

The Sn 3d was investigated of the H-SnTiO$_x$-E and H-CeSnTiO$_x$-E catalysts by XPS spectra and the result was presented in Fig. 7(d). The Sn $3d_{3/2}$ binding at lower energies for the H-SnTiO$_x$-E catalyst, illustrating that there were excess electrons around Sn [28,45]. It might be further explained a mass of Sn had incorporated into anatase TiO_2 and the existence of synergistic interaction between Ti and Sn, which could be agreed with XRD and Raman analysis. Moreover, for H-CeSnTiO$_x$-E catalyst, the Sn $3d_{3/2}$ binding energies was 494.9 eV as high as SnO_2, suggesting the Sn^{4+} was the primary valence state. In combination with XPS spectroscopy analysis of Ce, the synergistic interaction between Ce and Sn might exist through the redox equilibrium: $2Ce^{4+} + Sn^{2+} \leftrightarrow 2Ce^{3+} + Sn^{4+}$. Therefore, it could be confirmed that the ability of oxidation and reduction was remarkably improved in the ternary mixed metal oxide by adding Sn.

3.6. Surface acidities (NH_3-TPD)

Except as satisfactory redox performance, it was a pivotal factor that acid sites on the surface of catalyst were significant to improve the catalytic performance in NH_3- SCR reaction [45] and the NH_3-TPD

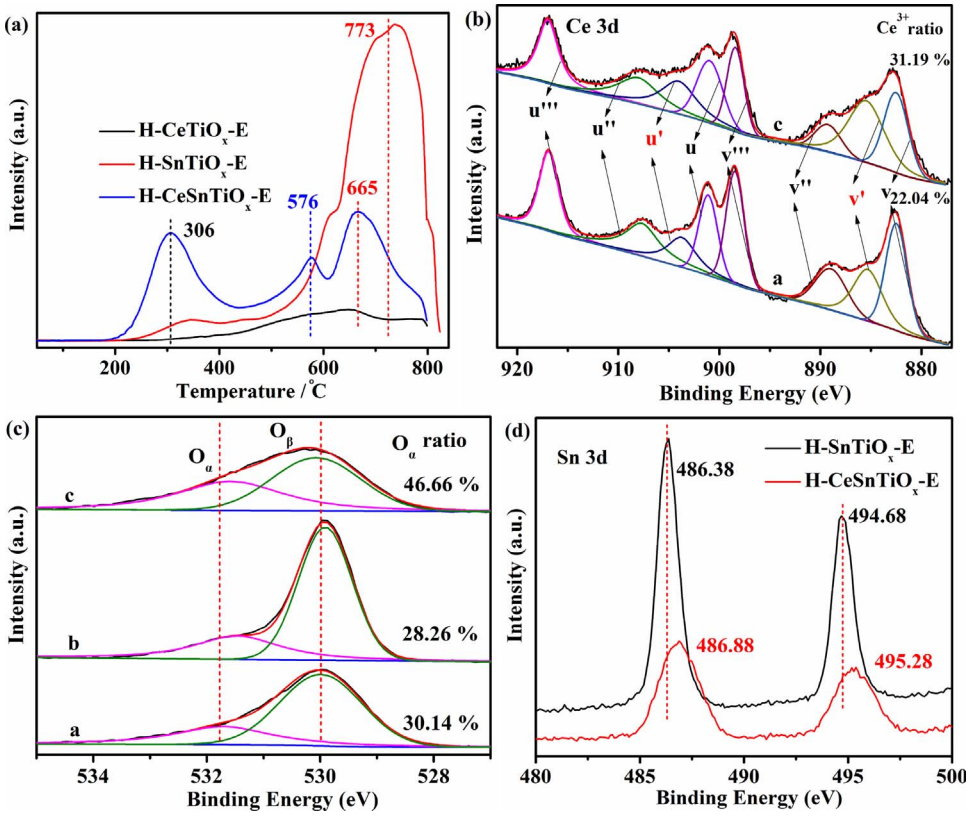

Fig. 7. H_2-TPR profiles (a) and Ce 3d (b), O 1s (c), Sn 3d (d) XPS spectra of the catalysts: H-CeTiO$_x$-E (a), H-SnTiO$_x$-E (b), H-CeSnTiO$_x$-E (c) catalysts.

Table 3
The surface atomic concentration and the peak-fitting results of O1s, Ce 3d spectra of the H-CeTiO$_x$-E, H-SnTiO$_x$-E and H-CeSnTiO$_x$-E catalysts.

Catalyst	Surface composition (at.%)				$O_\alpha/(O_\alpha + O_\beta) \times 100\%$	$Ce^{3+}/(Ce^{3+} + Ce^{4+}) \times 100\%$
	Ce	Sn	Ti	O		
H-CeTiO$_x$-E	23.17	–	5.76	71.08	30.14	22.04
H-SnTiO$_x$-E	–	7.62	22.12	70.26	28.26	–
H-CeSnTiO$_x$-E	9.51	5.48	14.14	70.87	53.34	31.19

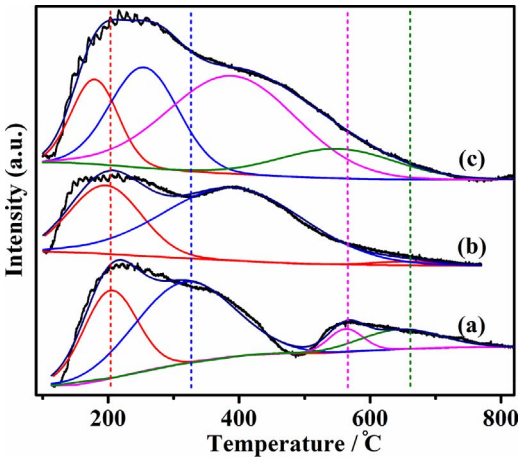

Fig. 8. NH_3-TPD profiles of the H-CeTiO$_x$-E (a), H-SnTiO$_x$-E (b) and H-CeSnTiO$_x$-E (c) catalysts.

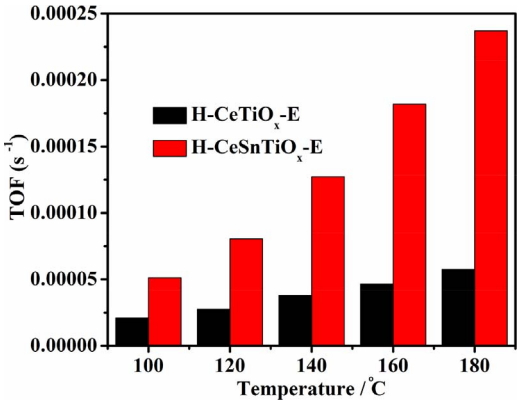

Fig. 9. The relative TOF profiles as a function of temperature over the H-CeTiO$_x$-E and H-CeSnTiO$_x$-E catalysts.

results were exhibited in Fig. 8. All the NH_3- TPD curves could be fitted and the information summarized in Table 4. As for the H-CeTiO$_x$-E catalyst, the curve was composed of two portions. The wide peak located below 350 ℃ was assigned to the weak and medium acid sites. Moreover, the peak at 520- 780 ℃ was attributed to the strong acid sites, which could adsorb NH_3 molecules [46–48]. In other words, the major Brønsted acid and limited Lewis acid sites participated in SCR reaction. On the contrary, for the H-SnTiO$_x$-E catalyst, the peak at 196 ℃ was attributed to the appearance of Brønsted acid sites and the peak located at 391 ℃ was assigned to Lewis acid sites, illustrating a handful of Brønsted acid and more Lewis acid sites existed. Obviously, the H-CeSnTiO$_x$-E catalyst not only possessed abundant Brønsted acid sites, but also provided adequate Lewis acid sites. It is concluded that the acid amount of the H-CeSnTiO$_x$-E catalyst was larger than that of others. All the peaks could be fitted and calculated and the regular was summarized below: H-CeSnTiO$_x$-E > H-SnTiO$_x$-E > H-CeTiO$_x$-E, indicating that surface acid sites were enhanced by doping tin. It was worth noting that Brønsted acid sites of the H-CeSnTiO$_x$-E catalyst were immensely improved, comparing with others, which be benefited to SCR reaction at low temperature. It could be confirmed that the NO conversion of the H-CeSnTiO$_x$-E catalyst was much higher than that of other catalysts.

3.7. The relative TOF calculation results

A relative turnover frequency (TOF) value was used to compare the catalytic velocity of different catalysts [38,49]. The TOF value of NO over per atom for the H-CeTiO$_x$-E and H-CeSnTiO$_x$-E catalysts were estimated according to Eq. (3) and corresponding profiles as a function of temperature were shown in Fig. 9. The TOF value of NO over the H-CeSnTiO$_x$-E catalyst was far higher than that of the H-CeTiO$_x$-E catalyst in the range of 100–180 ℃, demonstrating that per CeO_2 as active center reacted with NO. It is discovered that the superior activity of the H-CeSnTiOx-E catalyst was benefited from satisfactory specific surface area, uniformly pore channel and synergistic interaction between Ce and Sn.

3.8. Surface component and chemical states after enduring SO_2 test

To determine chemical states of the elements after enduring SO_2 test, the H-CeSnTiO$_x$-E catalyst was again investigated by XPS and the relevant information was summarized in Table 5. It was obvious that the surface atomic concentration of Ce and Sn decreased, while that of S and O increased, implying the surface of the catalyst was coated with a large amount of sulfur compounds after enduring SO_2 test. Especially, the surface S atomic concentration at 240 ℃ was far higher than that at 300 ℃, deducing that the catalyst was poisoned owing to plentiful sulfur compounds on the H-CeSnTiO$_x$-E catalyst surface.

Fig. 10(a) presented Ce 3d XPS spectra of the H-CeSnTiO$_x$-E catalyst

Table 4
The amount of surface acids over the H-CeTiO$_x$-E, H-SnTiO$_x$-E and H-CeSnTiO$_x$-E catalysts.

sample	Weak		Weak		Strong		Strong		Total
	T[a]	S[b]	T	S	T	S	T	S	S
H-CeTiO$_x$-E	205.6	937.7	322.9	1602.7	563.9	161.3	650.6	319.2	3020.9
H-SnTiO$_x$-E	195.6	1002.6	–	–	390.8	2109.2	656.2	47.8	3159.6
H-CeSnTiO$_x$-E	176.1	715.7	247.8	1398.4	385.8	2749.5	546.8	766.4	5630.0

[a] The peak at temperature (°C).
[b] Sum area (a.u.).

Table 5
The surface atomic concentration and the peak-fitting results of O1s, Ce 3d spectra of the H-CeSnTiO$_x$-E catalyst after enduring SO_2 test at 240 and 300 °C.

Catalyst	Surface composition (at.%)					$O_\alpha/(O_\alpha + O_\beta) \times 100\%$	$Ce^{3+}/(Ce^{3+} + Ce^{4+}) \times 100\%$
	Ce	Sn	Ti	O	S		
Fresh	9.51	5.48	14.14	70.87	–	53.34	31.19
240 °C	7.35	3.51	9.68	73.67	5.77	42.10	38.60
300 °C	3.04	3.95	17.16	72.72	3.13	58.60	36.61

after enduring SO_2 test at 240 °C (a) and 300 °C (b). Interestingly, the proportion of $Ce^{3+}/(Ce^{4+} + Ce^{3+})$ on these samples followed the order: fresh < 300 °C < 240 °C, demonstrating that there is the transformation between the valence states in the process of the reaction, such as $4Ce^{4+} + O^{2-} \rightarrow 4Ce^{4+} + 2e^- + 0.5O_2 \rightarrow 2Ce^{4+} + 2Ce^{3+} + 0.5O_2$ and $2Ce^{4+} + Sn^{2+} \leftrightarrow 2Ce^{3+} + Sn^{4+}$. The $Ce^{3+}/(Ce^{4+} + Ce^{3+})$ ratio after enduring SO_2 test at 300 °C was lower than that at 240 °C while the NO conversion stay around 85% and 60% over the H-CeSnTiO$_x$-E catalyst, respectively. We speculated the oxidation of Ce^{3+} could be restrained in the process, which would be also demonstrated by subsequent studies.

In addition to the obvious changes of Ce, it is notable that the chemical adsorption oxygen was distinctly different, as depicted in Fig. 10(b). Compared to the fresh catalyst, $O_\alpha/(O_\alpha + O_\beta)$ was transformed for H-CeSnTiO$_x$-E after enduring SO_2 test, which demonstrated a certain regular and summarized below: 240 °C < fresh < 300 °C. It was clear that there was a large amount of charge transfer between O^{2-} and Ce^{3+}. For the H-CeSnTiO$_x$-E catalyst after enduring SO_2 test at 240 °C, $O_\alpha/(O_\alpha + O_\beta)$ was much lower than that of fresh, while $Ce^{3+}/(Ce^{4+} + Ce^{3+})$ was higher than that of fresh, illustrating the process of reduction for Ce^{4+} was favorable to operating and the process of oxidation for Ce^{3+} was restrained. Moreover, SO_2 combined with Ce^{3+} to form more stable $Ce_2(SO_4)_3$, which could be hard to decompose. Hence, the efficiency greatly declined during the enduring SO_2 test at 240 °C. As for the H-CeSnTiO$_x$-E catalyst after enduring SO_2 test at 300 °C, $O_\alpha/(O_\alpha + O_\beta)$ and $Ce^{3+}/(Ce^{4+} + Ce^{3+})$ were much higher than that of fresh. It was efficient redox process for SCR reaction, O_α, Ce^{3+} and Ce^{4+} were kept in rational and regular status, thus ensuring the catalytic activity remained above 80%.

Remarkably, the binding energies of Sn (Fig. 10(c)) also changed, indicating that Sn was involved in SCR reaction. Binding energies of SnO_2 on the H-CeSnTiO$_x$-E catalyst after enduring SO_2 test at 240 °C was as high as that of fresh, suggesting the process of translation or conversion between Sn^{4+} and Ce^{3+} was prevented. Combining with above the Ce 3d and O 1s XPS studies, there were relatively higher Ce^{3+} and the lower O_α after the SO_2 enduring test at 240 °C than that of fresh catalyst. The low NO conversion was attributed to the formation of $Ce_2(SO_4)_3$, which was difficult to interact between SnO_2 and CeO_2. For the H-CeSnTiO$_x$-E catalyst after enduring SO_2 test at 300 °C, the Sn $3d_{3/2}$ binding energies were higher than that of fresh catalyst, indicating that tin participated in the oxidation process during the reaction. On the one hand, sulfur compounds were decomposed on the surface of the catalyst at 300 °C, allowing the reagent to contact the active center and sustaining SCR reaction. On the other, both the catalyst and reactant reached a high energy state, which facilitated the electron transfer of each metal element and promoted the reaction. Compared to the

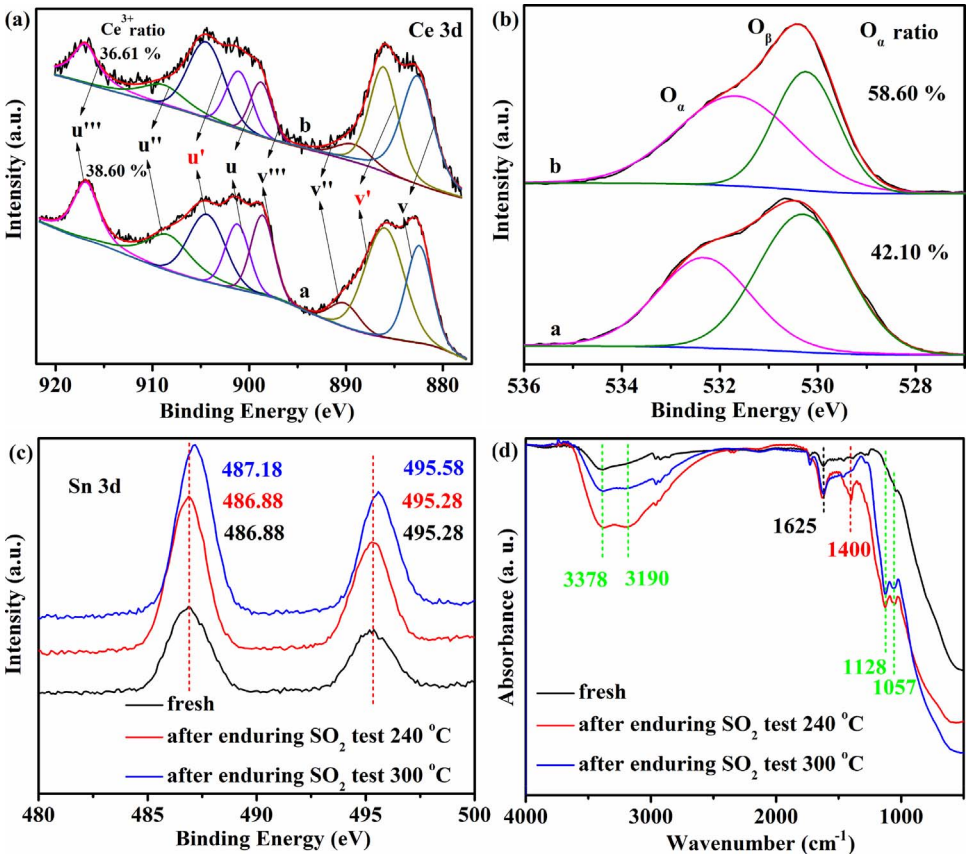

Fig. 10. Ce 3d (a), O 1s (b), Sn 3d (c) XPS spectra and FTIR results (d) of the H-CeSnTiO$_x$-E catalyst after enduring SO_2 test at 240 °C (a) and 300 °C (b).

previous literature [28,44], it was a key to promote the interaction of the metal elements by adding Sn.

To determine the products of catalyst surface after the SO_2 enduring test, H-CeSnTiO_x-E catalyst was investigated by FTIR and presented in Fig. 10(d). There were a few peaks for fresh catalyst and several of obvious peaks generated after SO_2 resistance tests. The bands at 1057 and 1128 cm^{-1} could be ascribed to NH_3 coordinated to Lewis acid sites and formed NH_4^+ species [50,51]. In the range of 1355–1420 cm^{-1} absorption peak corresponded to the typical deposited sulfate species of $\upsilon_{S=O}$. The wave number at 1625 cm^{-1} was assigned to bridging nitrate species [49,50]. Finally, the IR bands at 3190 and 3378 cm^{-1} were verified to N—H and O—H stretching vibration region [50,52–54]. Little bridging nitrate species and O—H stretching vibration region were detected for the fresh H-CeSnTiO_x-E catalyst, which meant a bit of H_2O adsorbed and the few nitrates undecomposed. For the H-CeSnTiO_x-E catalyst after enduring SO_2 test at 240 °C, in addition to above stronger and wider peaks, a mass of sulfate and NH_4^+ species were also observed, illustrating that $Ce_2(SO_4)_3$, $Ce(SO_4)_2$ and $(NH_4)_2SO_4$ were combined to the surface and covered the acid sites of the catalyst, which reduced the efficiency of SCR reaction. A little ammonium nitrate remained on the surface of the catalyst after enduring SO_2 test at 300 °C. Compared with our previous study [23], the resistance of SO_2 observably enhanced, which profited from improving the synergistic effect among the mixed metal oxides.

4. Conclusions

Sn modified ceria-titanium catalysts were prepared by solvothermal method and used in the SCR reaction of NO with NH_3. The H-CeSnTiO_x-E catalyst not only showed exceed 90% conversion at a wide range from 180 °C to 460 °C, but also exhibited satisfactory H_2O/SO_2 durability in the long term operation. It profited from better dispersion of active metal, strengthened the synergistic effect of metal particles, more crystal defects and oxygen vacancies, larger specific surface areas, uniform pore channel and improving acid sites. It was worth noting that the enhancement of electron interaction between Sn and Ce through the following redox equilibrium: $2Ce^{4+} + Sn^{2+} \leftrightarrow 2Ce^{3+} + Sn^{4+}$, which should be considered as the main reasons for the superior SCR performance and H_2O/SO_2 durability of the H-CeSnTiO_x-E catalyst. Finally, the deactivation reason was also investigated of H-CeSnTiO_x-E catalyst enduring SO_2 test at 240 °C, which could in further provide the strategy for design and synthesis of catalysts with H_2O and SO_2 tolerance at low temperature.

Acknowledgments

The authors acknowledge the support of Science and Technology Service Network Initiative (STS) of Chinese Academy of Science (KFJ-SW-STS-149), the National Basic Research Program of China (2013CB933201), the National Natural Science Foundation of China (21407154, 21507137) and Province Natural Science Foundation of GanSu (17jRSRA317).

Appendix A. Supplementary data

Supplementary data associated with this article can be found, in the online version, at https://doi.org/10.1016/j.apcatb.2017.12.030.

References

[1] W. Shan, F. Liu, H. He, X. Shi, C. Zhang, Appl. Catal. B: Environ. 115 (2012) 100–106.
[2] Y. He, M.E. Ford, M. Zhu, Q. Liu, U. Tumuluri, Z. Wu, I.E. Wachs, Appl. Catal. B: Environ. 193 (2016) 141–150.
[3] A.S. Negreira, J. Wilcox, J. Phys. Chem. C 117 (2013) 24397–24406.
[4] K. Zhao, W. Han, Z. Tang, G. Zhang, J. Lu, G. Lu, X. Zhen, Colloid Surf. A 503 (2016) 53–60.
[5] D. Klukowski, P. Balle, B. Geiger, S. Wagloehner, S. Kureti, B. Kimmerle, A. Baiker, J.-D. Grunwaldt, Appl. Catal. B: Environ. 93 (2009) 185–193.
[6] P. Zhang, H. Lu, Y. Zhou, L. Zhang, Z. Wu, S. Yang, H. Shi, Q. Zhu, S. Dai, Nat. Commun. 15 (2015) 1–10.
[7] J. Liu, X. Li, Q. Zhao, C. Hao, S. Wang, M. Tade, ACS Catal. 8 (2014) 2426–2436.
[8] S. Ding, F. Liu, X. Shi, H. He, Appl. Catal. B: Environ. 180 (2016) 766–774.
[9] J. Li, Y. Li, H. Peng, T. Chang, S. Zhang, W. Zhao, J. Si, Appl. Catal. B: Environ. 184 (2016) 246–257.
[10] D. Zhang, X. Du, L. Shi, R. Gao, Dalton Trans. 41 (2012) 14455–14475.
[11] G.G. Zaimes, B.J. Hubler, S. Wang, V. Khanna, ACS Sustain. Chem. Eng. 2 (2015) 237–244.
[12] K. Teramura, T. Tanaka, T. Funabiki, Langmuir 19 (2003) 1209–1214.
[13] Y. Gao, Y. Jiang, Y. Fu, Z. Zhong, K. Cen Luo, Catal. Commun. 11 (2010) 465–469.
[14] C. Tang, H. Zhang, L. Dong, Catal. Sci. Technol. 6 (2016) 1248–1264.
[15] Y. Gao, Y. Jiang, Z. Zhong, K. Luo, J. Cen, J. Hazard. Mater. 174 (2010) 734–739.
[16] F. Teocoli, D.W. Ni, S. Sanna, K. Thydén, F.C. Fonseca, V. Esposito, J. Mater. Chem. A 3 (2015) 17135–17143.
[17] B. Huang, R. Huang, D. Jin, D. Ye, Catal. Today 126 (2007) 279–283.
[18] G. Marbán, R. Antuña, A.B. Fuertes, Appl. Catal. B: Environ. 41 (2003) 323–338.
[19] R.Q. Long, R.T. Yang, Appl. Catal. B: Environ. 27 (2000) 87–95.
[20] W. Xu, H. He, Y. Yu, J. Phys. Chem. C 113 (2009) 4426–4432.
[21] P.G. Smirniotis, D.A. Pen, B.S. Uphade, Angew. Chem. Int. Ed. 40 (2001) 2479–2482.
[22] W. Shan, F. Liu, H. He, X. Shi, C. Zhang, Catal. Today 184 (2012) 160–165.
[23] G. Zhang, W. Han, F. Dong, L. Zong, G. Lu, Z. Tang, RSC Adv. 6 (2016) 76556–76567.
[24] E. Yuan, G. Wu, W. Dai, N. Guan, L. Li, Catal. Sci. Technol. 7 (2017) 3036–3044.
[25] D. Zhang, L. Zhang, L. Shi, C. Fang, H. Li, R. Gao, L. Huang, J. Zhang, Nanoscale 5 (2013) 1127–1136.
[26 F. Gu, S. Wang, C. Song, M. Lu, Y. Qi, G. Zhou, D. Xu, D. Yuan, Chem. Phys. Lett. 372 (2003) 451–454.
[27] G. Li, X. Zhang, S. Kawi, Sens. Actuators B 60 (1999) 64–70.
[28] L. Zhang, L. Li, Y. Cao, Y. Xiong, S. Wu, J. Sun, C. Tang, F. Gao, L. Dong, Catal. Sci. Technol. 5 (2015) 2188–2196.
[29] M. Yu, C. Li, G. Zeng, Y. Zhou, X. Zhang, Y. Xie, Appl. Surf. Sci. 342 (2015) 174–182.
[30] G. Busca, L. Liettib, G. Ramisa, F. Berti, Appl. Catal. B: Environ. 18 (1998) 1–36.
[31] L. Chen, J. Li, M. Ge, Environ. Sci. Technol. 44 (2010) 9590–9596.
[32] W. Shan, H. Song, Catal. Sci. Technol. 5 (2015) 4280–4288.
[33] K. Liu, F. Liu, L. Xie, W. Shan, H. He, Catal. Sci. Technol. 5 (2015) 2290–2299.
[34] K. Zhao, W. Han, G. Lu, J. Lu, Z. Tang, X. Zhen, Appl. Surf. Sci. 379 (2016) 316–322.
[35] R. Sui, J.L. Young, C.P. Berlinguette, J. Mater. Chem. 20 (2010) 498–503.
[36] Y. Gao, R. Li, S. Chen, L. Luo, T. Cao, W. Huang, Phys. Chem. Chem. Phys. 17 (2015) 31862–31871.
[37] C. Liu, L. Chen, J. Li, L. Ma, H. Arandiyan, Y. Du, J. Xu, J. Hao, Environ. Sci. Technol. 46 (2012) 6182–6189.
[38] C. Fang, D. Zhang, L. Shi, R. Gao, H. Li, L. Ye, J. Zhang, Catal. Sci. Technol. 3 (2013) 803–811.
[39] J.Z. Shyu, W.H. Weber, H.S. Gandhi, J. Phys. Chem. 92 (1988) 4964–4970.
[40] T. Baidya, A. Gupta, P.A. Deshpandey, G. Madras, M.S. Hegde, J. Phys. Chem. C 113 (2009) 4059–4068.
[41] K. Liu, L. Zhou, B. Wang, Y. Wang, J. Am. Chem. Soc. 131 (2009) 3140–3141.
[42] K. Krishna, A. Bueno-López, M. Makkee, J.A. Moulijn, Appl. Catal. B: Environ. 75 (2009) 201–209.
[43] B. Shen, Y. Wang, F. Wang, T. Liu, Chem. Eng. J. 236 (2014) 171–180.
[44] W. Xu, Y. Yu, C. Zhang, H. He, Catal. Commun. 9 (2008) 1453–1457.
[45] C. Fang, L. Shi, H. Li, L. Huang, J. Zhang, D. Zhang, RSC Adv. 6 (2016) 78727–78736.
[46] H. Yin, I. Han, A. Gunji, Endou S.S.C. Ammal, M. Kubo, A. Miyamoto, J. Phys. Chem. B 103 (1999) 4701–4706.
[47] R. Jin, Y. Liu, Z. Wu, H. Wang, T. Gu, Catal. Today 153 (2010) 84–89.
[48] H. Wang, X. Chen, X. Weng, Y. Liu, S. Gao, Z. Wu, Catal. Commun. 12 (2011) 1042–1045.
[49] J. Xue, X. Wang, G. Qi, J. Wang, M. Shen, W. Li, J. Catal. 297 (2013) 56–64.
[50] L. Zhang, L. Li, Y. Cao, X. Yao, C. Ge, F. Gao, Y. Deng, C. Tang, L. Dong, Appl. Catal. B: Environ. 165 (2015) 589–598.
[51] J. Wang, X. Dong, Y. Wang, Y. Li, Catal. Today 245 (2015) 10–15.
[52] H. Fu, X. Wang, H. Wu, Y. Yin, J. Chen, J. Phys. Chem. C 111 (2007) 6077–6085.
[53] W. Hu, Y. Zhang, S. Liu, C. Zheng, X. Gao, I. Nova, E. Tronconi, Appl. Catal. B: Environ. 206 (2017) 449–460.
[54] N. Chubar, V. Gerda, D. Banerjee, G. Yablokova, J. Colloid Interface Sci. 487 (2017) 388–400.